

# Independent control of beam astigmatism and ellipticity using a SLM for fs-laser waveguide writing

A. Ruiz de la Cruz, A. Ferrer, W. Gawelda, D. Puerto, M. Galván Sosa, J. Siegel, and J. Solís\*

*Laser Processing Group, Instituto de Optica, CSIC  
Serrano 121, Madrid, 28006, Spain  
\*j.solis@io.cfmac.csic.es*

**Abstract:** We have used a low repetition rate (1 kHz), femtosecond laser amplifier in combination with a spatial light modulator (SLM) to write optical waveguides with controllable cross-section inside a phosphate glass sample. The SLM is used to induce a controllable amount of astigmatism in the beam wavefront while the beam ellipticity is controlled through the propagation distance from the SLM to the focusing optics of the writing set-up. The beam astigmatism leads to the formation of two separate disk-shaped foci lying in orthogonal planes. Additionally, the ellipticity has the effect of enabling control over the relative peak irradiances of the two foci, making it possible to bring the peak irradiance of one of them below the material transformation threshold. This allows producing a single waveguide with controllable cross-section. Numerical simulations of the irradiance distribution at the focal region under different beam shaping conditions are compared to in situ obtained experimental plasma emission images and structures produced inside the glass, leading to a very satisfactory agreement. Finally, guiding structures with controllable cross-section are successfully produced in the phosphate glass using this approach.

©2009 Optical Society of America

**OCIS codes:** (130.3120) Integrated optics devices; (140.3390) Laser materials processing; (070.6120) Spatial light modulators; (220.4000) Microstructure fabrication.

---

## References and links

1. R. Osellame, V. Maselli, R. M. Vazquez, R. Ramponi, and G. Cerullo, "Integration of optical waveguides and microfluidic channels both fabricated by femtosecond laser irradiation," *Appl. Phys. Lett.* **90**(23), 231118 (2007).
2. G. D. Valle, R. Osellame, and P. Laporta, "Micromachining of photonic devices by femtosecond laser pulses," *J. Opt. A, Pure Appl. Opt.* **11**(1), 013001 (2009).
3. D. Day, and M. Gu, "Microchannel fabrication in PMMA based on localized heating by nanojoule high repetition rate femtosecond pulses," *Opt. Express* **13**(16), 5939–5946 (2005).
4. C. B. Schaffer, J. F. García, and E. Mazur, "Bulk heating of transparent materials using a high-repetition-rate femtosecond laser," *Appl. Phys., A Mater. Sci. Process.* **76**, 351–354 (2003).
5. V. Diez-Blanco, J. Siegel, A. Ferrer, A. R. D. L. Cruz, and J. Solís, "Deep subsurface waveguides with circular cross section produced by femtosecond laser writing," *Appl. Phys. Lett.* **91**(5), 051104 (2007).
6. A. Salimnia, N. T. Nguyen, M. C. Nadeau, S. Petit, S. L. Chin, and R. Vallée, "Writing optical waveguides in fused silica using 1 kHz femtosecond infrared pulses," *J. Appl. Phys.* **93**(7), 3724–3728 (2003).
7. G. Cerullo, R. Osellame, S. Taccheo, M. Marangoni, D. Polli, R. Ramponi, P. Laporta, and S. De Silvestri, "Femtosecond micromachining of symmetric waveguides at 1.5  $\mu\text{m}$  by astigmatic beam focusing," *Opt. Lett.* **27**(21), 1938–1940 (2002).
8. M. Ams, G. D. Marshall, D. J. Spence, and M. J. Withford, "Slit beam shaping method for femtosecond laser direct-write fabrication of symmetric waveguides in bulk glasses," *Opt. Express* **13**(15), 5676–5681 (2005).
9. J. Siegel, J. M. Fernández-Navarro, A. García-Navarro, V. Diez-Blanco, O. Sanz, J. Solís, F. Vega, and J. Armengol, "Waveguide structures in heavy metal oxide glass written with femtosecond laser pulses above the critical self-focusing threshold," *Appl. Phys. Lett.* **86**(12), 121109 (2005).
10. G. D. Love, "Wave-front correction and production of Zernike modes with a liquid-crystal spatial light modulator," *Appl. Opt.* **36**(7), 1517–1520 (1997).

11. R. R. Thomson, A. S. Bockelt, E. Ramsay, S. Beecher, A. H. Greenaway, A. K. Kar, and D. T. Reid, "Shaping ultrafast laser inscribed optical waveguides using a deformable mirror," *Opt. Express* **16**(17), 12786–12793 (2008).
12. M. Pospiech, M. Emons, A. Steinmann, G. Palmer, R. Osellame, N. Bellini, G. Cerullo, and U. Morgner, "Double waveguide couplers produced by simultaneous femtosecond writing," *Opt. Express* **17**(5), 3555–3563 (2009).
13. C. Mauclair, G. Cheng, N. Huot, E. Audouard, A. Rosenfeld, I. V. Hertel, and R. Stoian, "Dynamic ultrafast laser spatial tailoring for parallel micromachining of photonic devices in transparent materials," *Opt. Express* **17**(5), 3531–3542 (2009).
14. Y. Igasaki, F. Li, N. Yoshida, H. Toyoda, T. Inoue, N. Mukohzaka, Y. Kobayashi, and T. Hara, "High Efficiency Electrically-Addressable Phase-Only Spatial Light Modulator," *Opt. Rev.* **6**(4), 339–344 (1999).
15. M. Born, and E. Wolf, *Principles of Optics* (Cambridge University Press, 1997).
16. G. Zhao, X. Ji, and B. Lu, "Approximate analytical propagation equations of Gaussian beams through hard-aperture optics," *Optik (Stuttg.)* **114**(6), 241–245 (2003).
17. W. Gawelda, D. Puerto, J. Siegel, A. Ferrer, A. Ruiz De La Cruz, H. Fernández, and J. Solis, "Ultrafast imaging of transient electronic plasmas produced in conditions of femtosecond waveguide writing in dielectrics," *Appl. Phys. Lett.* **93**(12), 121109 (2008).

## 1. Introduction

Non-linear processing of dielectrics with ultrashort laser pulses has enabled the production of a variety of functional elements in microfluidics and integrated optics, including micro-channels, optical waveguides, amplifiers, and lasers [1–3]. The transversal cross-section of the written structures is a key parameter for the performance of the fabricated devices. Its control is conditioned, among other parameters, by the repetition rate of the writing laser. In the high repetition rate regime ( $f \geq 100$  kHz) [4], material modification is affected by heat accumulation and later diffusion, favoring the production of structures with a circularly symmetric cross-section. In the low frequency regime (typically  $f \approx 1$  kHz), the absence of cumulative heat effects, the characteristics of Gaussian beam propagation and the presence of spherical aberration effects, lead to structures with a cross-section that is elongated along the beam propagation axis [5,6]. This problem can be partially overcome by the use of elliptical beams, generated using either cylindrical telescopes [7] or slits [8]. The focal volume can then be shaped as a thin disk, and translating the sample transversally to the focal disk yields structures with circular cross section. However, these approaches offer a limited flexibility for handling processing conditions influenced by severe aberration effects. This is the case in materials with a large index of refraction (e.g. heavy metal oxide glasses [9]) or when using focusing optics with high numerical apertures beyond a certain processing depth, where spherical aberration has a substantial effect on the focal volume geometry [5]. This can be particularly relevant when the irradiation conditions (writing direction and depth) are dynamically modified during the writing process (e.g. production of 3D structures).

The use of spatial light modulators (SLMs), either deformable mirrors or liquid crystal based, provides in turn a flexible and energy-efficient alternative for shaping the focal volume [10,11]. Additionally it enables the pre-compensation of optical aberrations, and the use of multiplexing or the self-adaptive writing schemes [12,13]. Particularly, the work in Ref [11] uses a deformable mirror to shape the writing beam. The mirror acts as a variable cylindrical mirror, focusing the beam along one axis in order to generate an elliptical beam with an aspect-ratio at the focusing optics similar to that produced by slit-shaping [8]. Still, SLMs are not completely free of constraints, such as the effects of phase wrapping in liquid crystal SLMs or of cross-talk in deformable mirrors.

In this work we have used a liquid-crystal SLM to modify the wavefront of the writing beam in order to control the transversal aspect ratio of structures produced in glass with fs laser pulses. By inducing a given amount of astigmatism in the beam and controlling the propagation distance between the SLM and the writing optics it is feasible to achieve this goal. After focusing, the astigmatic beam leads to the formation of two flat-shaped sagittal and tangential foci. We demonstrate that by correctly setting the propagation distance of the astigmatic beam before focusing, the relative peak irradiances of the two foci can be controlled. We also identify the conditions to efficiently suppress one of them, while using the other to write a single light-guiding structure with controllable cross-section.

## 2. Experimental set-up

The experimental set-up used is shown in Fig. 1. It is based on a Ti:Sapphire chirped pulse amplifier (Spectra-Physics Spitfire), delivering  $\lambda = 800$  nm laser pulses with a duration  $\tau \approx 100$  fs, a repetition rate  $f = 1$  kHz, and a maximum pulse energy  $E = 1$  mJ. An optically addressed PAL-SLM (Hamamatsu X8267-14DB, reflectivity at 800 nm,  $R_{800\text{nm}} \approx 90\%$  [14], ) modifies the beam wavefront. The SLM applies a static correction to compensate the initial beam aberrations (wavefront distortion compensated to  $< 0.12 \mu\text{m}$  p.v.) and induces a known amount of astigmatism, using the corresponding phase-map. The astigmatic aberration induced in the beam at the SLM surface is characterized by the Zernike coefficient corresponding to the desired aberration [10] as experimentally measured with a Hartmann-Shack wavefront sensor (Imagine Optic HASO 76) after image-relaying the SLM plane to the input plane of the HASO (at very weak irradiance). The aberrated beam is subsequently propagated through a controllable distance ( $d = 80$ -170 cm) using a trombone arrangement before being focused inside a glass sample (undoped MM2 phosphate glass from Kigre Inc.) using a microscope objective (20X, numerical aperture  $\text{NA} = 0.4$ , focal length  $f = 10$  mm, entrance pupil diameter  $\phi = 8$  mm). In what follows, the laser pulse energy values quoted correspond to measurements performed right after the focusing objective.

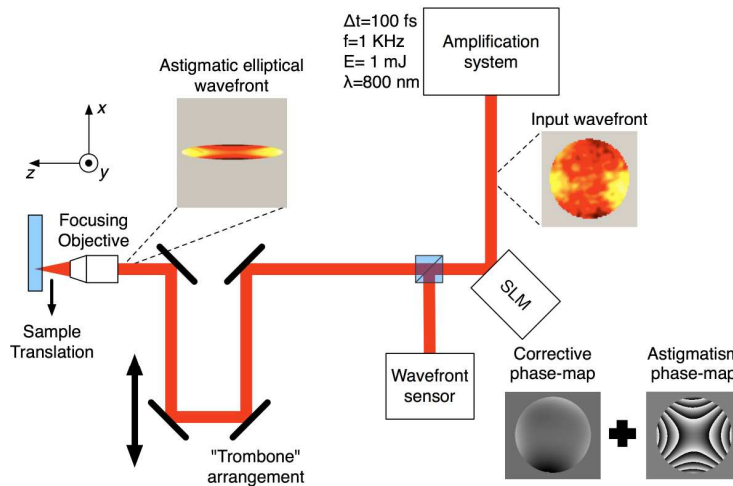


Fig. 1. Experimental set-up used for optical waveguide writing controlling the astigmatism and ellipticity of the irradiation beam with a SLM. It shows an image of the wavefront before the SLM and the phase-maps used to correct the initial aberrations and induce a given amount of astigmatism to the beam. The ellipticity of the beam is controlled by the propagation distance using the trombone arrangement.

## 3. Effect of astigmatism

Figure 3(a)–3(c) shows several images of calculated irradiance cross section along  $y$ - $z$  plane (according to the geometry of Fig. 1) of the irradiance distribution in the focal region for increasing values of astigmatism ( $Z_4$  Zernike coefficient) for a propagation distance  $d = 80$  cm. The value of  $Z_4$  is defined for a circular pupil size of 7 mm ( $1/e^2$  diameter of the incident beam on the SLM). It represents the peak wavefront deformation of the beam. The calculations were performed using the ABCD matrix formalism for the propagation of a Gaussian elliptical astigmatic beam [5,15]. This code includes the effect of propagation from the SLM surface to the input plane of the focusing optics and diffraction effects at the entrance pupil of the focusing objective [16] due to clipping of the beam when overfilling the pupil.

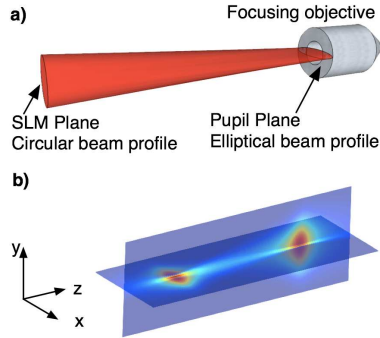


Fig. 2. Schematic drawing of the astigmatism and beam propagation effects on the beam profile at the entrance pupil of the focusing objective (a) and on the irradiance distribution in the focal region, showing two foci lying in orthogonal planes (b).

The combined effect of astigmatism and propagation leads to an astigmatic elliptical beam at the entrance pupil of the focusing optics. This is schematically depicted in Fig. 2. As shown (Fig. 2(a)), the focusing optics is overfilled along the  $x$ -axis and under-filled along the  $y$ -axis (for positive values of  $Z_4$ ). As a consequence of the beam astigmatism, the irradiance distribution in the focal region (Fig. 2(b)), shows two disk-shaped foci lying on orthogonal planes ( $x$ - $z$  and  $y$ - $z$ ) and located in front and behind the position of the paraxial focus. We will refer to them from now on as first and second focus respectively.

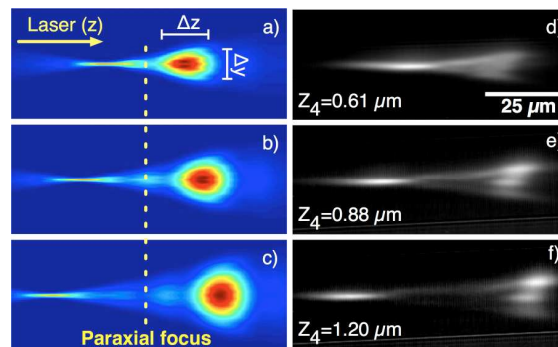


Fig. 3. Numerically calculated cross-sections of the irradiance distribution ( $y$ - $z$  plane) after propagating and focusing a beam inside a glass sample for various astigmatism values ( $Z_4$ ). The parameters used are: objective NA = 0.4, propagation distance  $d = 80$  cm, focal length  $f = 10$  mm and depth  $z = 300$   $\mu\text{m}$  (a)-(c). Images of plasma emission generated by focusing an astigmatic beam in a phosphate glass sample with the same parameters as the numerical calculations, for pulses with energy  $E = 300$  nJ (d)-(f).

Figure 3(a)-3(c) shows, the calculated irradiance distribution in the focal region for various values of astigmatism for an objective NA of 0.4, a propagation distance of 80 cm and a focusing depth of 300  $\mu\text{m}$ . As expected, the separation between the two foci increases with the amount of aberration, while at the same time the aspect ratio  $R = \Delta z/\Delta y$  (ratio of the focus dimensions along the  $z$  and  $y$  axis) decreases. The same figure (Fig. 3(d)-3(f)) also shows experimental plasma emission images corresponding to the same NA, propagation distance, and beam astigmatism values. The images were obtained with a transverse microscopy setup [17] after focusing the beam under static conditions inside a phosphate glass sample. In order to avoid both cumulative damage and non-linear propagation effects, the energy of the excitation pulses was maintained at 0.3  $\mu\text{J}$  while the beam was focused at a processing depth of  $z = 300$   $\mu\text{m}$ . The plasma images also show a three-lobe irradiance distribution, most likely caused by phase wrapping effects at the SLM. This happens when the required wavefront distortion is beyond the maximum continuous phase shift achievable by our SLM (4.2 radians), therefore making it necessary to use a wrapped phase-map distribution.

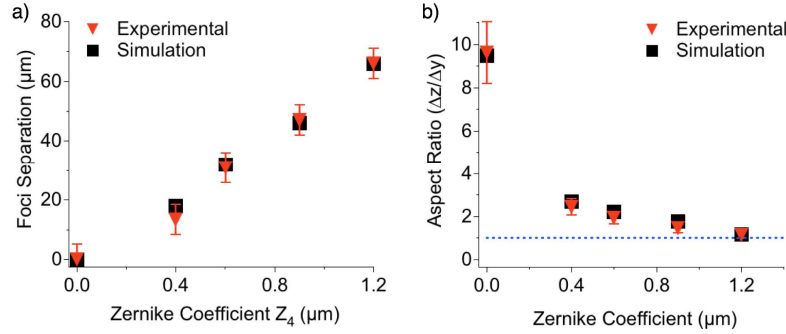


Fig. 4. Plots representing the separation between foci (a) and aspect ratio ( $\Delta z/\Delta y$ ) of the cross-section for the second focus (b) as a function of astigmatism in the irradiation beam wavefront. The fixed parameters used are:  $d = 80$  cm,  $z = 300$   $\mu\text{m}$  and  $f = 10$  mm.

The plot in Fig. 4(a) displays experimental and calculated values for the separation distance between the first and second focus as a function of astigmatism ( $Z_4$ ) using the same parameters as in Fig. 3. The experimental data were obtained from plasma emission images (see Fig. 3(d)-3(f)). The error bars shown are associated to the fact that, in absence of non-linear propagation effects, each focus has a Gaussian irradiance distribution. Accordingly we have estimated the error in the foci separation to be of the order of the Rayleigh range of the beams ( $\approx 10$   $\mu\text{m}$ ). The agreement between simulated and experimental data is very good, showing a linear scaling. The aspect ratio of the second focus ( $R_{zy} = \Delta z/\Delta y$  using the axis defined in Fig. 2) as a function of astigmatism is plotted in Fig. 4(b). In this case, the error bars included relate (among other factors) to the uncertainty in the determination of the aspect ratio of the plasma emission images caused by phase wrapping effects. We estimate the error in the measurement of the aspect ratio to be around 15%. In the figure, we also observe a very good agreement between model and experiment, showing that  $R_{zy}$  can be controlled, from  $R_{zy} > 6$  to  $R_{zy} \approx 1$  for  $0 \leq Z_4 \leq 1.2$   $\mu\text{m}$ . A comparison with the parameters used in Ref [11] would have been interesting; unfortunately, the authors do not provide values of the applied wavefront deformation. Moreover, their approach to beam shaping modifies the beam along a single axis, whereas our approach (using astigmatism) allows control of the beam over both  $x$  and  $y$ -axis. In addition, the use of astigmatism gives a more reliable set of parameters ensuring the reproducibility of the obtained results.

#### 4. Effect of propagation distance

Modeling also enables us to assess in detail the effect of the propagation distance on the beam irradiance at the focal region. The induced astigmatism has the effect of changing the ellipticity of the beam as it propagates. For a given value of  $Z_4$  the beam will become more elliptical with an increasing propagation distance. For our experimental set-up geometry (see Fig. 1), the propagated beam will be stretched along the horizontal direction ( $x$ -axis) and compressed along the vertical direction ( $y$ -axis), affecting the effective numerical aperture of the focusing optics along each direction and thus the irradiance of each astigmatic focus. The results can be seen in Fig. 5(a)-5(d), showing the calculated  $y$ - $z$  and  $x$ - $z$  cross-sections of the beam irradiance distribution in the focal region, for parameters similar to those used in Fig. 3(c) ( $Z_4 = 1.4$   $\mu\text{m}$ ) but for propagation distances  $d = 0.1$  m (Fig. 5(a)-5(b)) and  $d = 1.73$  m (Fig. 5(c)-5(d)).

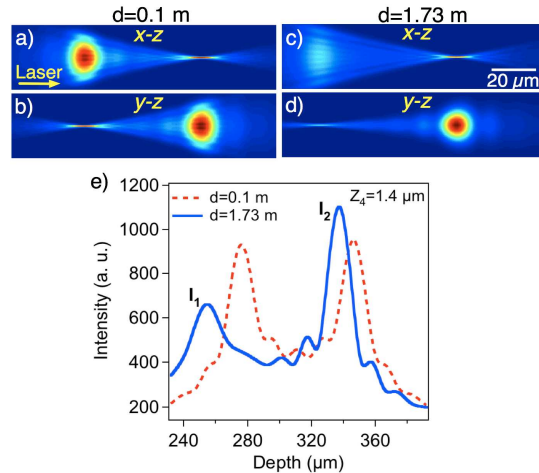


Fig. 5. Numerical calculations of the irradiance distribution for an astigmatic beam in the focal region ( $f = 10$  mm,  $z = 300$   $\mu\text{m}$  and pupil diameter of focusing optics  $\phi = 8$  mm) for propagation distances  $d = 0.1$  m (a)-(b) and  $d = 1.73$  m (c)-(d); irradiance profiles along the  $z$ -axis for both propagation distances (e).

Because of the combined effect of astigmatism and ellipticity, the relative peak irradiance ratio between the first and second focus changes with the propagation distance. A plot of the calculated irradiance profiles along the  $z$ -axis for the same astigmatism value, and the two indicated propagation distances ( $d = 0.1$  and  $d = 1.73$  m) is shown in Fig. 5(e). It is clear, that for the astigmatic elliptical beam with longer propagation distance ( $d = 1.73$  m), the peak irradiance at the first focus is approximately a factor of two smaller than the one corresponding to the second focus, while for an astigmatic beam with little ellipticity ( $d = 0.1$  m, short propagation distance) both foci show the same peak irradiance. Adjusting  $d$  allows us to smoothly control the relative irradiance ratio between the two foci. Consequently, by setting the peak irradiance at the first focus ( $I_1$ , in Fig. 5(e)) below the transformation threshold, it is then possible to modify the material only at the second one ( $I_2$ , in Fig. 5(e)). Figure 6(a)-6(b) shows optical microscopy cross-section images of two structures written with the same astigmatism value  $Z_4 = 1.2$   $\mu\text{m}$ , propagation distance  $d = 1.73$  cm, depth  $z = 300$   $\mu\text{m}$ , NA = 0.4 and scanning speed  $v = 100$   $\mu\text{m/s}$  for two different pulse energies  $E = 3$   $\mu\text{J}$  and  $E = 1.2$   $\mu\text{J}$ . In Fig. 6(a) there are two structures corresponding to both astigmatic foci due to the irradiance at both being above the modification threshold for the material. In order to leave the first focus below threshold and suppress it, we lowered the energy to 1.2  $\mu\text{J}$ . The image in Fig. 6(b) shows a single structure at the position corresponding to the second focus as predicted by our numerical calculations.

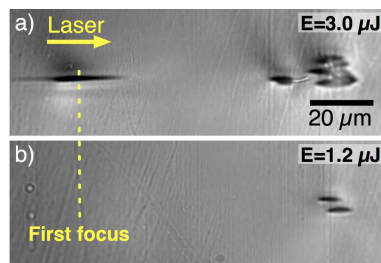


Fig. 6. Optical microscopy cross-section images of structures written with the following parameters:  $f = 10$  mm,  $\phi = 8$  mm,  $Z_4 = 1.2$   $\mu\text{m}$ ,  $d = 1.73$  m,  $z = 300$   $\mu\text{m}$  and  $v = 100$   $\mu\text{m/s}$ , for two different irradiation energies  $E = 3.0$   $\mu\text{J}$  (a) and  $E = 1.2$   $\mu\text{J}$  (b).

Finally, we have used the approach described in this work to write a guiding structure inside a phosphate glass sample. Figure 7(a) shows the transillumination image of a

waveguide inscribed using five writing scans with the following parameters:  $Z_4 = 1.4 \mu\text{m}$ ,  $d = 1.73 \text{ m}$ ,  $z = 300 \mu\text{m}$ ,  $f = 10 \text{ mm}$ ,  $\phi = 6 \text{ mm}$  energy per pulse  $E = 1.0 \mu\text{J}$ . The bright regions in the image show a lobular structure, similar to those of the plasma images in Fig. 3. However, a near-field image of the guided mode at  $\lambda = 633 \text{ nm}$  shown in Fig. 7(b) presents a single guided mode with a desired symmetric shape (aspect ratio  $R = 1$ ). Furthermore, the dark regions to both sides of the bright ones are most likely zones where the refractive index of the material has decreased. This hypothesis is consistent with the observation that the confinement of the mode in the guiding image of Fig. 7(b) appears stronger along the horizontal axis, where the dark regions in Fig. 7(a) lie.

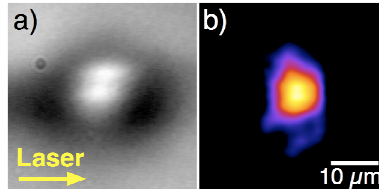


Fig. 7. Transillumination microscope image of a waveguide fabricated with an astigmatic beam ( $Z_4 = 1.4 \mu\text{m}$ ,  $E = 1.0 \mu\text{J}$ ,  $d = 1.73 \text{ m}$ ,  $z = 300 \mu\text{m}$  and  $v = 100 \mu\text{m/s}$ ) and five writing scans (a). Near-field guided-mode image of the same waveguide for  $\lambda = 633 \text{ nm}$  (b).

## 5. Conclusion

In conclusion, structures with controllable transversal cross-section have been written in a phosphate glass sample using astigmatic elliptical beams produced by a SLM. The aspect ratio is controlled by the value of induced astigmatism, producing two structures corresponding to each of the foci of the astigmatic beam. Adjusting the propagation distance between the SLM and the focusing objective, allows control over the ellipticity of the astigmatic beam, which translates into different relative peak irradiances between both foci. This allows us to use a propagation distance such that only the second one is above the transformation threshold of the material, completely suppressing the structure created with the first focus.

## Acknowledgements

This work was partially supported by the Spanish Ministry of Science and Innovation under TEC2008-01183 project. A. R. and W. G. acknowledge their I3P-CSIC postdoctoral contracts (co-funded by the European Social Fund). D. P. and A. F. acknowledge their grants under Projects TEC 2005-00074 and TEC 2006-04538.